IEEE Access
Multidisciplinary | Rapid Review | Open Access Journal

Received June 16, 2020, accepted June 30, 2020, date of publication July 10, 2020, date of current version August 4, 2020.

Digital Object Identifier 10.1109/ACCESS.2020.3008156

3D Transient Electromagnetic-Temperature Field Analysis of the Loss and Heat of the Damper Bars of a Large Tubular Hydro-Generator During Short Circuit Faults

QING-LING HU[1], KE XIAO[1], ZHI-TING ZHOU[2], ZHEN-NAN FAN[1], YONG YANG[3], ZU-YING BIAN[1], JING-CAN LI[2], AND BING YAO[1]

[1]The Key Laboratory of Fluid and Power Machinery, Ministry of Education, Xihua University, Chengdu 610039, China
[2]State Key Laboratory of Power Transmission Equipment and System Security and New Technology, Chongqing University, Chongqing 400030, China
[3]Research and Test Center, Dongfang Electric Machinery Company, Ltd., Deyang 618000, China

Corresponding author: Zhen-Nan Fan (fanzhennan@126.com)

This work was supported in part by the National Natural Sciences Fund Youth Fund of China, under Grant 51607146 and Grant 61703345; in part by the Key Scientific Research Fund Project of Xihua University, under Grant Z1520907 and Grant Z1520909; in part by the Key Research Fund Projects of Sichuan Provincial Education Department, under Grant 16ZA0155 and Grant 16ZB0159; in part by the Sichuan Science and Technology Program, under Grant 2018GZ0391; in part by the Chunhui Project Foundation of the Education Department of China, under Grant Z2016144; in part by the Open Research Subject of Key Laboratory of Fluid and Power Machinery (Xihua University), Ministry of Education, Xihua University, Chengdu, China, under Grant SZJJ2015-027; and in part by the Altair Provides FLUX Software Support.

ABSTRACT This paper studies a real 36-MW large tubular hydro-generator to solve the transient variation problem of the loss and heat of damper bars during short circuit faults in tubular hydro-generators. The transient analysis method of electromagnetic-temperature fields is adopted to study the transient variation problem of the loss and heat of damper bars during three-phase symmetrical short-circuits, single-phase to ground asymmetrical short-circuits, and phase-to-phase asymmetrical short-circuits under rated operation states. The research work provides valuable findings for improving the level of state analysis, the design and manufacturing processes, and the operation and maintenance of large-scale tubular hydro-generators.

INDEX TERMS Damper bar, loss and heat, short-circuit, 3D transient electromagnetic-temperature field analysis, tubular hydro-generator.

I. INTRODUCTION

Although damper windings are the key components for ensuring the safe and stable operation of hydro-generators, their state has a vital impact on the operational safety of generators. Especially, during dangerous and special conditions, such as short circuits, negative sequences, etc., the loss and heat state of damper windings greatly affect their safe and stable operation, the generator, and the whole power grid.

With the development of medium and high head water energy resources being almost completed, more attention is paid to the development of low head water energy resources. In comparison with hydro-generators in medium and high water heads, which are operated using impulse-type, mixed-flow-type, and axial-low-type turbines, tubular hydro-generators are best for developing and utilizing low water head rivers and tidal water energy resources, saving 20-30% of civil construction costs and increasing power generation by 3-5% [1], [2]. However, as there is a large number of poles in such generators and due to the space restrictions resulting from their flow channels and the hydraulic performance of their bulb bodies, the stator and rotor diameters and the air gaps of these generators are significantly smaller than those of other hydro-generators. Thus, in case of a short-circuit fault, the damper windings are likely to face a severe loss and a heat impact, and their safety status becomes worse. Especially for the current level of power system protection technology in China, although in most situations, the relay protection device can remove the fault within 0.5 seconds or even less after the generator short-circuit fault. As a matter of fact, for the most of

The associate editor coordinating the review of this manuscript and approving it for publication was Mehmet Alper Uslu.

the tubular hydro-generators (the capacity is usually below 50MW), due to the imperfect configuration of their relay protection device, the backup protection often takes 3 to 4 seconds or even longer to remove the fault in the case of failure of the main protection. If the more extreme failure of the relay protection device occurs, the time to remove the fault will be longer. Under these situations, the loss and heat of damper winding will be more serious. Therefore, it is necessary to establish a relevant physical field analysis model to carry out a more comprehensive and in-depth study on the transient variation problem of the loss and heat of damper bars during short circuits in such hydro-generators.

However, up till now, although researchers have carried out a series of studies on the current, magnetic field, electromagnetic force, impedance, and stator heating of hydro-generators during short circuits [3]–[9], research work on the transient analysis of the electromagnetic and temperature fields responsible for the loss and heat transient process of damper windings of tubular hydro-generators during short-circuit faults has yet to be developed further.

This paper aims to solve the above-mentioned problems by studying the operation of a 36-MW large tubular hydro-generator as an example. For its three typical short-circuit fault conditions, namely, the three-phase symmetrical short circuit, the single-phase to ground asymmetrical short circuit, and the A-B phase asymmetrical short-circuit, the transient state of the loss and heat of damper windings during the above-mentioned faults is studied through the analysis and calculation of transient electromagnetic and temperature fields. The research work provides valuable findings for improving the state analysis, the design and manufacturing processes, and the operation and maintenance of large-scale tubular generators.

II. CALCULATION MODELS

A. GENERATOR PARAMETERS

The specifications and basic data of the generator (SFWG36-72/7350) in this study are listed in TABLE 1.

TABLE 1. The basic data of generator.

Parameter	Value
Rated power (MW)	36
Rated voltage (V)	10.5
Rated current(A)	2151
Power Factor	0.92
Number of poles	72
Number of damper bars per pole	4
Number of stator slots per pole per phase	1½
Stator slot skewed degree	0.5slot

B. MULTI-SLICE MOVING ELECTROMAGNETIC FIELD-CIRCUIT COUPLING MODEL OF THE GENERATOR

The influence of the skewed stator slot structure was analyzed to form a multi-slice moving electromagnetic field-circuit coupling model of the generator [10].

According to the periodicity of the generator's magnetic field, a pair of poles was chosen as the electromagnetic field calculation region. Based on the stator slot skewed structural design, the generator was divided into twelve equal slices along the axial direction as shown in Fig. 1.

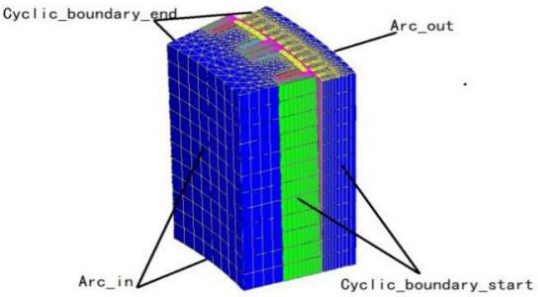

FIGURE 1. Problem regions and FE meshes of electromagnetic fields.

Considering the saturation of an iron core, the 3D boundary value problem of a nonlinear time-varying moving electromagnetic field was obtained as follows,

$$\begin{cases} \nabla \times (\nu \nabla \times \mathbf{A}) + \dfrac{1}{\rho}\left[\dfrac{\partial \mathbf{A}}{\partial t} - \mathbf{V} \times (\nabla \times \mathbf{A})\right] = \mathbf{J}_s \\ \mathbf{A}\,|_{Arc\_in} = \mathbf{A}\,|_{Arc\_out} = 0 \\ \mathbf{A}\,|_{Ccylic\_boundary\_start} = \mathbf{A}|_{Ccylic\_boundary\_end} = 0, \end{cases} \tag{1}$$

where $\mathbf{A}$ is the magnetic vector potential, $\mathbf{J_s}$ is the source current density, ν is the reluctivity, $\mathbf{V}$ is the velocity, and ρ is the resistivity.

For each slice, the current density and magnetic vector potential only have the axial z component, and the speed only has the circumferential x component. With the Coulomb norm $\cdot\ \mathbf{A} = 0$ and the boundary condition of the problem region, the 2D boundary value problem of the nonlinear time-varying moving electromagnetic was then obtained as follows,

$$\begin{cases} \dfrac{\partial}{\partial x}\left(\nu \dfrac{\partial A_{slz}}{\partial x}\right) + \dfrac{\partial}{\partial y}\left(\nu \dfrac{\partial A_{slz}}{\partial y}\right) = -J_{slz} + \dfrac{1}{\rho}\dfrac{\partial A_{slz}}{\partial t} \\ \qquad + \dfrac{V_x}{\rho}\dfrac{\partial A_{slz}}{\partial x} \\ A_{slz}|_{arc\_in} = A_{slz}|_{arc\_out} = 0 \\ A_{slz}|_{cyclic\_boundary\_start} = A_{slz}|_{cyclic\_boundary\_end} \end{cases} \tag{2}$$

where V_x is the circumferential component of the velocity, J_{slz} is the axial component of the source current density, and A_{slz} is the magnetic vector potential.

To consider the influence of the stator end winding and the rotor damper winding end rings and the excitation winding, the coupling circuit models were then established as discussed in the literature [11]–[13]. The coupling circuit is shown in Fig. 2.

According to the circuit law, the coupled circuit equations can be obtained,then,the coupling circuit equations and the electromagnetic field equations are combined, the magnetic vector potential A_{slz} of the slices can be calculated by the time-step FE method. Thus, the stator and rotor winding currents and the damper bars eddy current losses (the heat sources of the damper bars) can be acquired.

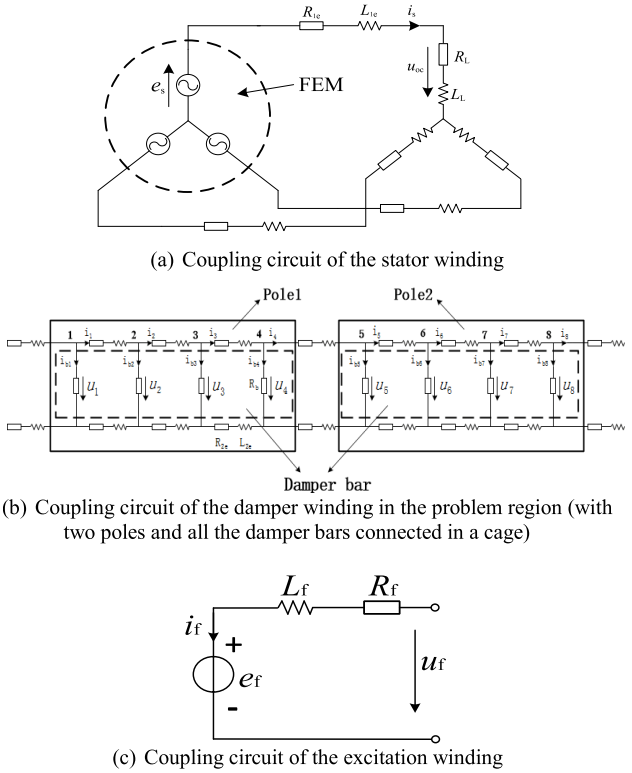

(a) Coupling circuit of the stator winding

(b) Coupling circuit of the damper winding in the problem region (with two poles and all the damper bars connected in a cage)

(c) Coupling circuit of the excitation winding

FIGURE 2. Coupling circuit.

It should be noted that the details of the above field-circuit coupling model are shown in the APPENDIX I of this paper.

C. BOUNDARY VALUE PROBLEM OF THE ROTOR 3D TRANSIENT TEMPERATURE FIELD

Because of the symmetrical ventilation air cooling structure of this generator, half the axial section of the rotor pole is selected as the problem region for the 3D temperature field solving as shown in Fig. 3. There are 4 damper bars on each pole shoe. So, for an easier discussion, the damper bar on the leeward side is numbered as the 1st, and the damper bar on the windward side is numbered as the 4th.

Then, considering the anisotropic heat conduction condition of the rotor core, the boundary value problem of the 3D transient temperature field can be expressed as follows,

$$\begin{cases} \dfrac{\partial}{\partial x}(\lambda_x \dfrac{\partial T}{\partial x}) + \dfrac{\partial}{\partial y}(\lambda_y \dfrac{\partial T}{\partial y}) + \dfrac{\partial}{\partial z}(\lambda_z \dfrac{\partial T}{\partial z}) + q_V = \rho c \dfrac{\partial T}{\partial t} \\ \lambda \dfrac{\partial T}{\partial n}\Big|_{S_A} = 0 \\ \lambda \dfrac{\partial T}{\partial n}\Big|_{S_B} = -\alpha(T - T_f), \end{cases} \tag{3}$$

where T is the temperature, $\lambda_x, \lambda_y, \lambda_z$ represent the heat conductivity on each direction, respectively, q_v is the heat source density, which is obtained by the above-mentioned multi-slice moving electromagnetic field-circuit coupling model of the generator, ρ is the density of the material, c is material specific heat, S_A represents the rotor middle profile and the interface between the rotor core and the rim related to the thermal insulation boundary condition, S_B is the outside surface of the rotor related to the heat dissipation boundary condition, α is the heat dissipation coefficient of S_B, and T_f is the environment air temperature.

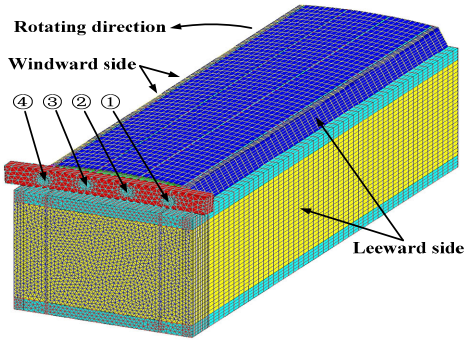

FIGURE 3. Problem region of 3D temperature field.

On this basis, a time-step FE analysis of the 3D transient temperature field is carried out so the time-varying trend of the damper bar temperature can be obtained.

It should be noted that the details of the above 3D transient temperature field model are shown in the APPENDIX I of this paper.

III. CALCULATION RESULTS AND ANALYSIS

A. CALCULATION PARAMETER SETTING

In this study, the three-phase load resistance and inductance in the coupling circuit are first set as the rated values, which are used to calculate the loss of the generator's damper bar under the rated condition. They are also used as the initial heat source (the heat source of the damper bar before the short-circuit fault) to solve the transient temperature field of the damper bar under the short-circuit fault condition. On this basis, in the coupled circuit, three kinds of short-circuit fault conditions are respectively set: three-phase symmetrical short-circuit, A-phase single-phase to ground short-circuit, and A-B phase asymmetrical short-circuit. Then, through the transient time-step FE calculation of the electromagnetic field, the relevant damper bar loss is solved, which is used as a heat source for solving the transient temperature field of the damper bar during the above-mentioned three fault conditions.

Moreover, according to the current level of relay protection technology in China, in case of a short-circuit fault in a generator, the fault is removed within 0.5 seconds under the normal operation of the main protection. However, if the main protection fails to remove the fault, it can still be removed within 3-4 seconds by the back-up protection. Thus, we set the upper time limit of the transient temperature field analysis to 4 seconds after the short circuit.

In addition, it is important to mention that the accuracy and rationality of the above calculation model are partially verified by the damper bar temperature test data. And the damper bar temperature test details are shown in the APPENDIX II of this paper.

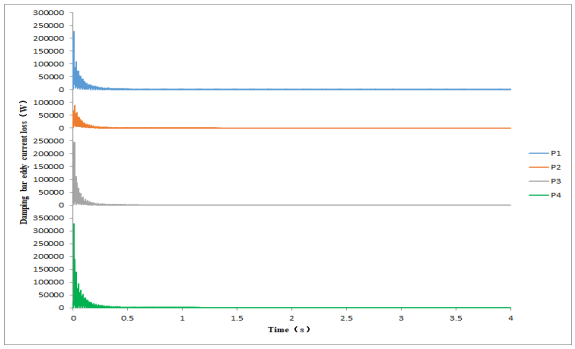

(a) Three-phase symmetrical short circuit

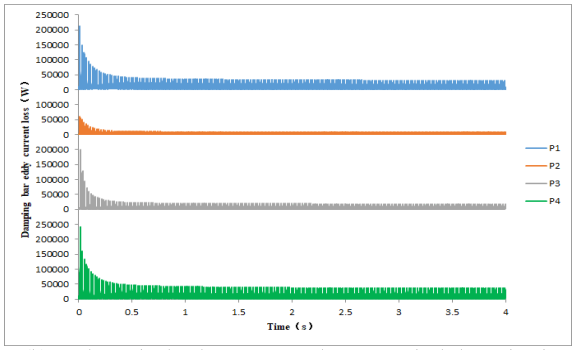

(b) A-phase single-phase to ground asymmetrical short circuit

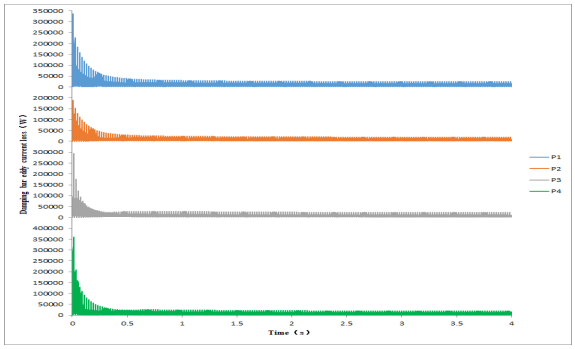

(c) A-B phase asymmetrical short circuit

FIGURE 4. Transient curve of the damper bar loss after the short circuit.

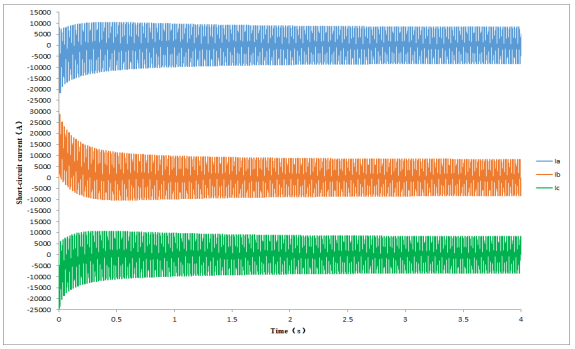

(a) Three-phase symmetrical short circuit

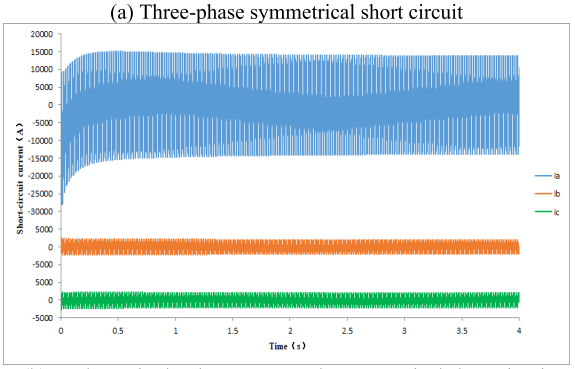

(b) A-phase single-phase to ground asymmetrical short circuit

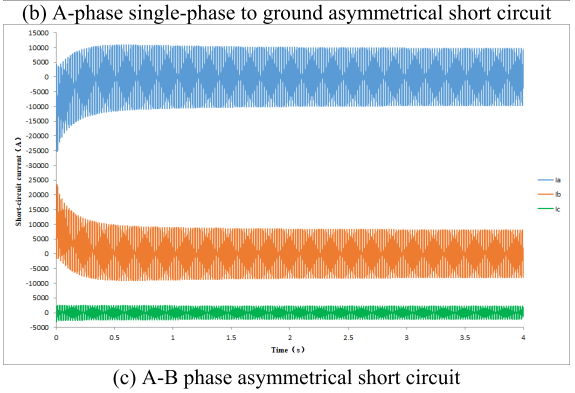

(c) A-B phase asymmetrical short circuit

FIGURE 5. Transient curve of the stator current after the short circuit.

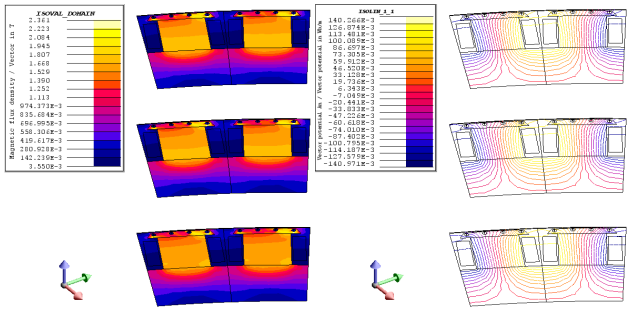

FIGURE 6. Distribution of the generator's magnetic field before the short circuit (rated symmetrical operation condition).

B. DAMPER BAR LOSS RESULTS

Through the time-step finite element analysis of the transient electromagnetic field, the transient curve of the damper bar loss after the short circuit is shown in Fig. 4. The relevant stator current and the generator magnetic field distribution are represented in Fig. 5–9. In addition, some important loss values are shown in Table 2–5. It should also be noted that, in this study, the rotation direction of the generator's pole is counter-clockwise. In addition, in order to make the magnetic field distribution more clearly displayed on the computer screen, in Fig. 6–9, only the upper, middle, and lower three layers of the multi-slice model are displayed.

C. ANALYSIS OF THE DISTRIBUTION LAW OF THE DAMPER BAR LOSS ACCORDING TO THE LAW OF THE MAGNETIC FIELD

From the above results, the following phenomena were deducted:

First, in terms of the above three typical short-circuit faults, the loss of the four damper bars in the damper windings in a single pole went from a sharp increase to attenuation and finally to a stable condition within 4 seconds after the occurrence of the short-circuit. Specifically, 0.5 seconds after

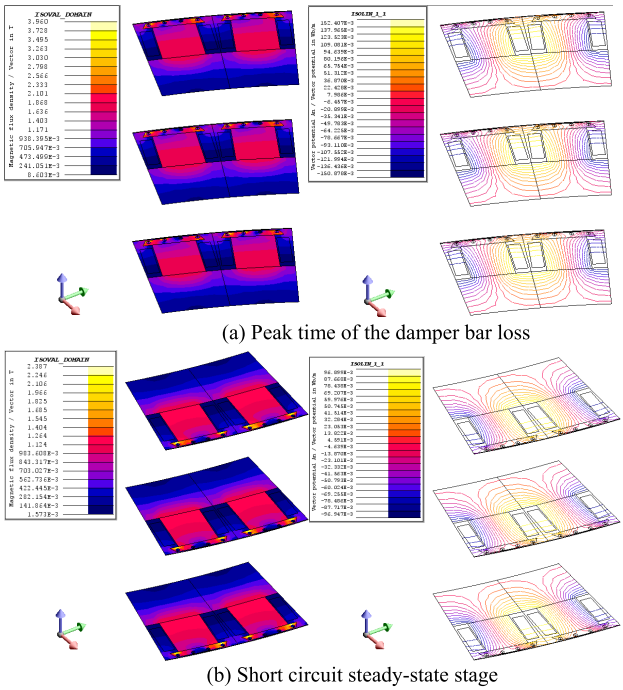

(a) Peak time of the damper bar loss

(b) Short circuit steady-state stage

FIGURE 7. Generator magnetic field distribution (three-phase symmetrical short circuit).

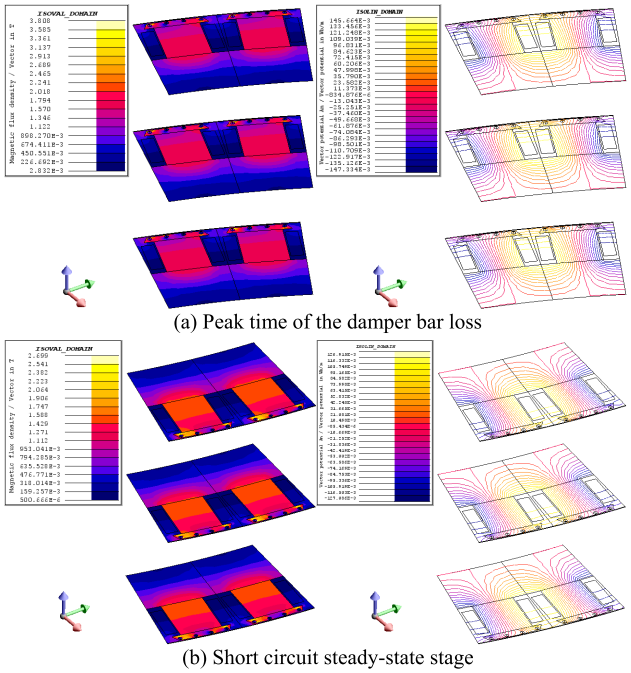

(a) Peak time of the damper bar loss

(b) Short circuit steady-state stage

FIGURE 8. Generator magnetic field distribution (A-phase single-phase to ground asymmetrical short circuit).

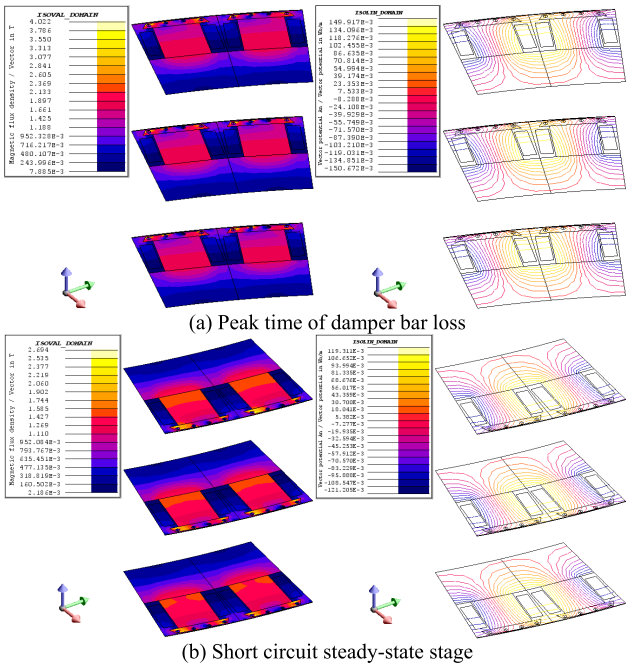

(a) Peak time of damper bar loss

(b) Short circuit steady-state stage

FIGURE 9. Generator magnetic field distribution (A-B phase asymmetrical short circuit).

TABLE 2. Damper bar loss (befor short circuit).

	Loss (W)			
	P_1	P_2	P_3	P_4
Steady state value	635	308	141	70

TABLE 3. Damper bar loss (three-phase symmetrical short circuit).

	Loss (W)			
	P_1	P_2	P_3	P_4
Peak value	226739	87429	245777	327920
Steady state value	469	331	308	447

TABLE 4. Damper bar loss (A-Phase Single-Phase to ground asymmetrical short circuit).

	Loss (W)			
	P_1	P_2	P_3	P_4
Peak value	211204	60895	199169	241008
Steady state value	10523	3130	5273	11672

the occurrence of the short-circuit, the damper bar loss curve decayed into a stable state as shown in Fig. 4. In addition, its peak value could even reach the order of 3.2×10^5W. The reason is that, during the short circuit, the stator current shows the trend from the sharp increase to the attenuation and then to the stable condition as shown in Fig. 5. Therefore, the eddy current loss induced in the damper bar should also show similar behavior.

Secondly, after the short-circuit fault, the loss distribution law of the damper bars significantly changes. Specifically, before the short-circuit, the loss of the first and second damper bars near the leeward area of the pole was far

TABLE 5. Damper bar loss (A-B phase asymmetrical short-circuit).

	Loss (W)			
	P_1	P_2	P_3	P_4
Peak value	336217	189601	293928	360362
Steady state value	11102	7774	8212	8597

greater than that of the third and fourth damper bars near the windward area of the pole. Also, the loss of the first damper bar was the largest. However, when the above-mentioned three short-circuit fault conditions occurred, the loss of the first and fourth damper bars near the pole edge was far greater than that of the second and third damper bars near the pole centerline. In particular, the loss of the third and fourth damper bars close to the windward side significantly increased, where the loss of the fourth damper bar, which is closest to the windward side, reached or even exceeded that of the first damper bar.

The reasons for such phenomena are as follows. Before the short-circuit fault, the generator was in the rated operation state, where, as shown in Fig. 6, the magnetic field distribution in its pole area inclined to the leeward side, the magnetic field in the leeward side was significantly stronger than that in the windward side, and the magnetic density in the leeward side was also much higher than that in the windward side. However, after the short-circuit fault, the magnetic field in the windward side of the pole was significantly enhanced, and its magnetic density reached or even exceeded that of the leeward area as shown in Fig. 7–9. The above variation trend of the magnetic field distribution has a direct impact on the eddy current losses induced in the damper bar, making it have similar properties and a similar distribution law.

Thirdly, in general, the loss of the damper bar in the above two asymmetrical short circuit conditions is much greater than that in the three-phase symmetrical short circuit condition. The reason is that when the above two kinds of asymmetric short-circuit faults occur, it is as if the generator is connected to a huge transient asymmetric load. Thus, the strong negative sequence magnetic field induces more eddy current losses in the damper bar.

D. ANALYSIS OF THE DAMPER BAR TEMPERATURE RESULTS

On the basis of the above 3D electromagnetic -temperature field time-step FE analysis, the temperature distribution and time-varying conditions of the damper bar after the above three types of short-circuit faults are obtained as shown in Fig. 10-14 and Table 6–8. It should be noted that in the Fig.14, ΔT_1, ΔT_2, ΔT_3 and ΔT_4 represent the temperature rise of the first to fourth damper bar respectively.

According to the above results, while taking into consideration the data in TABLE 2–IV in section B, it was found that the temperature state of the damper bar shows the following phenomena after the short-circuit faults.

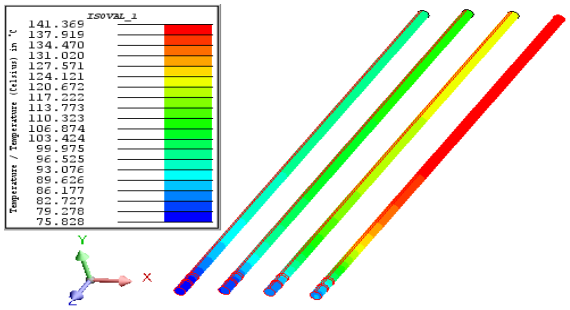

FIGURE 10. Temperature distribution of the damper bar (before the short circuit).

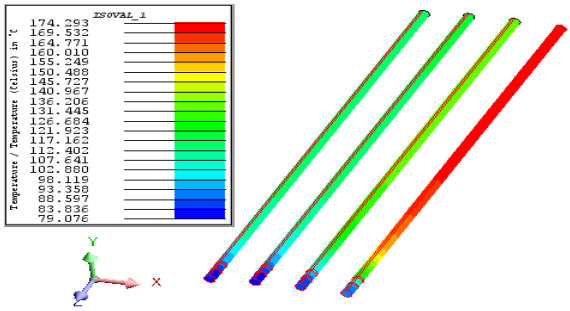

FIGURE 11. Temperature distribution of the damper bar (4 seconds after the three-phase symmetrical short circuit).

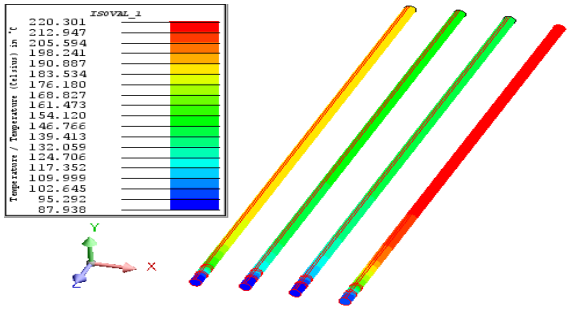

FIGURE 12. Temperature distribution of the damper bar (4 seconds after the A-phase single-phase to ground asymmetrical short circuit).

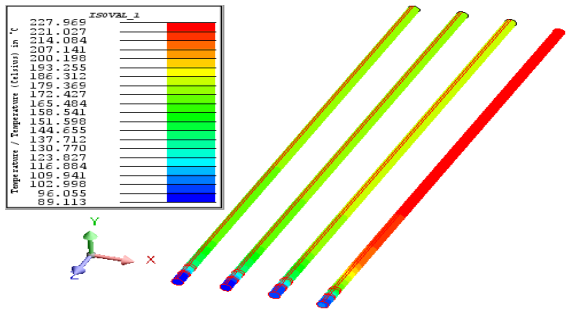

FIGURE 13. Temperature distribution of the damper bar (4 seconds after the A-B phase asymmetrical short circuit).

First, the temperature of the damper bar is highest during the A-B phase asymmetrical short circuit fault, followed by that during the A-phase single-phase to ground asymmetrical short circuit, and the temperature during the three-phase symmetrical short circuit is lowest. Obviously, this is determined by the heat source of the damper bar in the above fault condition.

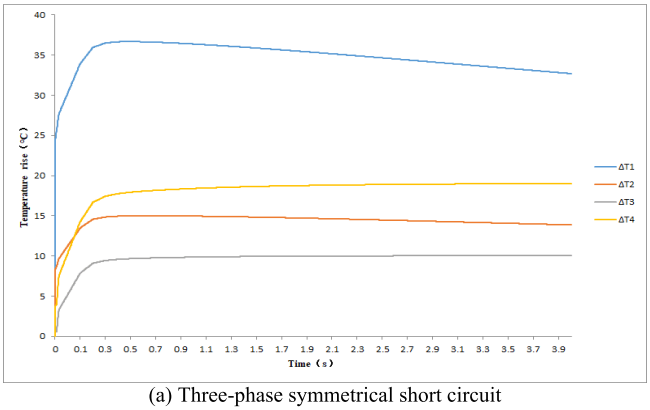

(a) Three-phase symmetrical short circuit

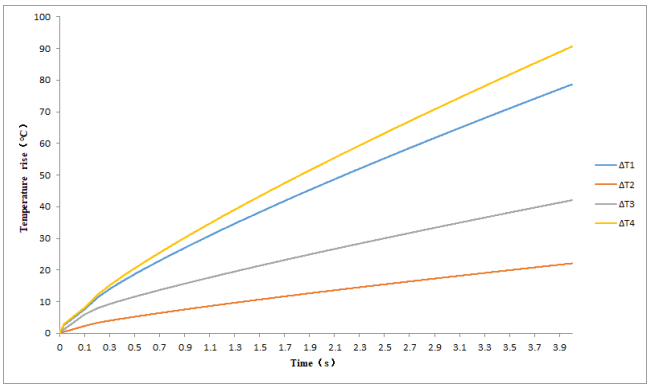

(b) A-phase single-phase to ground asymmetrical short circuit

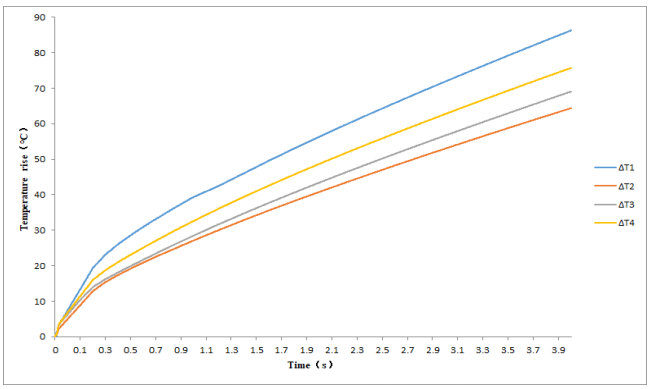

(c) A-B phase asymmetrical short circuit

FIGURE 14. Temperature rise curve of the damper bar.

TABLE 6. Temperature rise value of the damper bar (three-phase symmetrical short circuit).

	Damper bar			
	1	2	3	4
T_{max}(℃)	174	135	118	118
T_{min}(℃)	141	122	108	98
$\Delta T=T_{max}-T_{min}$(℃)	33	13	10	20

Secondly, the highest temperature of the damper bar still takes place in the middle of the first damper bar. There are three reasons for this phenomenon, and they are described as follows. Before the short circuit, the loss and temperature of the first damper bar was significantly higher than that of the other three damper bars. Then, after the short circuit, the loss of the first damper bar was still high. Besides, the first damper bar is closest to the leeward side of the pole, which has poor heat dissipation.

TABLE 7. Temperature rise value of the damper bar (A-Phase single-phase to ground asymmetrical short circuit).

	Damper bar			
	1	2	3	4
T_{max}(℃)	220	144	150	189
T_{min}(℃)	141	122	108	98
$\Delta T=T_{max}-T_{min}$(℃)	79	22	42	91

TABLE 8. Temperature rise value of the damper bar (A-B phase asymmetrical short circuit).

	Damper bar			
	1	2	3	4
T_{max}(℃)	228	186	177	174
T_{min}(℃)	141	122	108	98
$\Delta T=T_{max}-T_{min}$(℃)	87	64	69	76

Thirdly, the temperature rise of the fourth damper bar is much higher than that of the third and second damper bars. However, its maximum temperature may not be higher than that of each of the former two bars. There are two reasons for this phenomenon. First, after the short circuit, the loss of the fourth damper bar was far greater than that of the second and third bars, and it was close to or even more than that of the first bar. Therefore, the heat source determines if each bar has a relatively large temperature rise. Secondly, before the short circuit, the loss and temperature of the fourth damper bar were lowest. Besides, the fourth damper bar is closest to the pole's windward side, so its heat dissipation is relatively good. Therefore, although the temperature rise of the fourth damper bar is far greater than that of the second and third bars due to the sharp increase in the loss after the short circuit, its maximum temperature may not be higher than that of each of the former two bars.

In addition, more attention needs to be paid to the following phenomena. After experimenting with the above two kinds of asymmetric short circuits, even though the loss of the damper bar greatly decreased to a stable value in a short time, the temperature of the damper bar was still far from stable, and it continued to rise. Only 4 seconds after the asymmetrical short circuit, the maximum temperature rise of the damper bar exceeds 90°C. Thus, if the fault cannot be removed on time, a higher temperature rise takes place, threatening the safety of damper bar, and the pole iron core, and the insulation material, even the operational safety of the generator and the power grid.

IV. CONCLUSION

In this paper, we aim to solve the transient variation problem of the loss and heat of damper bars in tubular hydro-generators during short-circuit faults. The electromagnetic-temperature field transient analysis method was used to study the loss and heat transient evolution trend of the generator's damper bars during three typical short-circuit faults in its rated operation: three-phase symmetrical short-circuit, A-phase single-phase to ground asymmetrical short-circuit, and A-B phase asymmetrical short-circuit. The following conclusions were then drawn.

① After the short-circuit fault, the loss distribution of the damper bar has the following characteristics. Primarily, the loss of the damper bar near the pole edge is far greater than that near the pole centerline. Secondly, the loss of the third and fourth damper bars near the windward side of the pole greatly increases, and the loss of the fourth damper bar, which is closest to the windward side, most significantly increases, reaching or even exceeding the loss of the first damper bar, which is closest to the leeward side. Thirdly, the loss of the damper bar in the asymmetric short circuit is much greater than that in the symmetric short circuit.

② After the short circuit fault, the temperature state of the damper bar has the following characteristics. At first, the first damper bar, which is closest to the leeward side of the pole, has the highest temperature. Besides, although the temperature of the fourth damper bar, which is closest to the windward side, may not be higher than that of each of the second and third damper bars, its temperature rise is significantly higher than that of each of them.

③ Thirdly, more attention needs to be paid to the following phenomena. After experimenting with the above two kinds of asymmetric short circuits, even though the loss of the damper bar greatly decreased to a stable value in a short time, the temperature of the damper bar was far from stable, and it continued to rise substantially. Especially in the current power system of China, for some tubular Hydro-generator with imperfect protection device, when the above fault occurs, if the main protection fails, the fault removal time maybe even longer than that mentioned in this paper. Under this situation, the temperature of the damper bar is likely to be much higher than that mentioned in this paper, which will probably cause damage to the damper bar. It can be seen that although the capacity of tubular Hydro-generator is not very large, it must be equipped with perfect relay protection facilities to avoid the above damage.

④ In fact, because the short-circuit condition of the generator in this paper is a very serious fault condition, the hydropower plant will not allow us to recover the fault and measure the temperature through the site test as this will undoubtedly cause serious damage to the generator. So in this paper, the physical field model is only partially verified for normal working conditions(as shown in the APPENDIX II of this paper). In order to further verify the 3D FE analysis results of this paper, we will try to persuade some generator manufacturers in China to further verify the analysis model and results of this paper by means of factory test or simulation. We prepare to use a new paper for further discussion.

⑤ In the current situation with lack of direct measurement results, the research of this paper is helpful for the generator designers to master the distribution and change law of the damper winding loss and heat in the case of short circuit of the tubular hydro-generator. Therefore, it can help improve the level of the design and protection configuration of this kind of generator.

⑥ In addition, it is noteworthy that currently generator manufacturers in china are designing and manufacturing the giant hydro-generators with single unit capacity of 1000MW. The design parameters of such giant hydro-generators have exceeded the design limits of any hydro-generators in the past. Therefore, higher requirements are proposed for the safe operation of damper winding and even the whole generator. At the same time, the loss and heat transient variating law of damper winding of such a giant Hydro-generator under short-circuit fault cannot be obtained directly by actual measurement, because it will bring unacceptable damage to the generator,and causing great economic loss. Therefore, using the 3D transient electromagnetic field - temperature field analysis model in this paper to evaluate the loss and heat of the damper winding under the short-circuit condition will undoubtedly provide a relatively reasonable technical support and engineering reference for the design and manufacture of such giant Hydro-generator. This is what we are going to do in the future. We are planning to use a new paper for special discussion.

APPENDIX I
THE DETAILS OF MODELS

A. THE DETAILS OF MULTI-SLICE MOVING ELECTROMAGNETIC FIELD-CIRCUIT COUPLING MODEL OF THE GENERATOR

The influence of the skewed stator slot structure was analyzed to form a multi-slice moving electromagnetic field-circuit coupling model of the generator [10].

According to the periodicity of the generator's magnetic field, a pair of poles was chosen as the electromagnetic field calculation region. Based on the stator slot skewed structural design, the generator was divided into twelve equal slices along the axial direction as shown in Fig. 1.

Considering the saturation of an iron core, the 3D boundary value problem of a nonlinear time-varying moving electromagnetic field was obtained as follows,

$$\begin{cases} \nabla \times (v\nabla \times \mathbf{A}) + \dfrac{1}{\rho}\left[\dfrac{\partial \mathbf{A}}{\partial t} - \mathbf{V} \times (\nabla \times \mathbf{A})\right] = \mathbf{J}_s \\ \mathbf{A}\,|_{Arc\_in} = \mathbf{A}\,|_{Arc\_out} = 0 \\ \mathbf{A}\,|_{Ccylic\_boundary\_start} = \mathbf{A}|_{Ccylic\_boundary\_end} = 0, \end{cases} \tag{A-1-1}$$

where $\mathbf{A}$ is the magnetic vector potential, $\mathbf{J_s}$ is the source current density, v is the reluctivity, $\mathbf{V}$ is the velocity, and ρ is the resistivity.

For each slice, the current density and magnetic vector potential only have the axial z component, and the speed only has the circumferential x component. With the Coulomb norm $\cdot \mathbf{A} = 0$ and the boundary condition of the problem region, the 2D boundary value problem of the nonlinear time-varying moving electromagnetic was then obtained as follows,

$$\begin{cases} \dfrac{\partial}{\partial x}\left(\nu\dfrac{\partial A_{slz}}{\partial x}\right)+\dfrac{\partial}{\partial y}\left(\nu\dfrac{\partial A_{slz}}{\partial y}\right)=-J_{slz}+\dfrac{1}{\rho}\dfrac{\partial A_{slz}}{\partial t} \\ \qquad +\dfrac{V_x}{\rho}\dfrac{\partial A_{slz}}{\partial x} \\ A_{slz}|_{arc\_in}=A_{slz}|_{arc\_out}=0 \\ A_{slz}|_{cyclic\_boundary\_start}=A_{slz}|_{cyclic\_boundary\_end} \end{cases} \tag{A-1-2}$$

where V_x is the circumferential component of the velocity, J_{slz} is the axial component of the source current density, and A_{slz} is the magnetic vector potential.

To consider the influence of the stator end winding and the rotor damper winding end rings and the excitation winding, the coupling circuit models were then established as discussed in the literature [11]–[13]. The stator coupling circuit is shown in Fig. 2(a). The stator winding parallel branch number is one for each slice. Therefore, the voltage equation of the stator circuit is

$$e_s = u_{oc} + R_{1e}i_s + L_{1e}\frac{di_s}{dt}, \tag{A-1-3}$$

where e_s, $u_{oc,}$ and i_s are the inductive EMF, the voltage, and the current of the stator phase winding, respectively. R_{1e} and L_{1e} are the resistance and the leakage inductance of the stator end winding, respectively, R_L is the resistance of the load, and L_L is the inductance of the loads.

In the rotor of this tubular hydro-generator, there are 4 damper bars on each pole. The considered problem region in this study consists of only two poles. Thus, there are 8 damper bars in total. Fig. 2(b) shows the circuit of the damper bars in the problem region for every slice as previously demonstrated in the literature [11], where all the damper bars are connected in a cage.

Supposing that i_{k-1} and i_k are the end ring currents on the left and right branches of kth damper bar, respectively, the relationship between i_{k-1}, i_k and the current of the damper bar i_{bk} can be obtained:

$$i_k - i_{k-1} + i_{bk} = 0 \tag{A-1-4}$$

Then, the voltage equation that describes the relationship between the kth and (k + 1)th branches of the damper bars is

$$u_k - u_{k+1} = 2i_kR_{2e} + 2L_{2e}\frac{di_k}{dt}, \tag{A-1-5}$$

where R2e and L2e are the resistance and the inductance of the damper winding end ring, respectively.

From the periodic condition, the constraint conditions of the current and the voltage on the boundary are

$$\boldsymbol{i}_1 + \boldsymbol{i}_n + \boldsymbol{i}_{b1} = \mathbf{O} \tag{A-1-6}$$

$$u_n - u_1 = 2i_nR_{2e} + 2L_{2e}\frac{di_n}{dt}, \tag{A-1-7}$$

where n is the number of damper bars in the problem region. When n is 8, the following equations are obtained:

$$\boldsymbol{i}_1 + \boldsymbol{i}_8 + \boldsymbol{i}_{b1} = \mathbf{O} \tag{A-1-8}$$

$$u_8 - u_1 = 2i_8R_{2e} + 2L_{2e}\frac{di_8}{dt} \tag{A-1-9}$$

The coupling circuit of the excitation winding of the hydro-generator is shown in Fig. 2(c).

The excitation winding loop equation is shown in equation (10) as follows,

$$u_f = e_f + i_fR_f + L_f\frac{di_f}{dt}, \tag{A-1-10}$$

where e_f is the induced electromotive force of the excitation winding, u_f is the excitation winding voltage, i_f is the excitation winding current, R_f is the excitation winding resistance, and L_f is the excitation winding inductance.

If the stator and rotor coupling circuit equations and the electromagnetic field equations are combined, the magnetic vector potential A_{slz} of the slices can be calculated by the time-step FE method. Thus, the stator and rotor winding currents and the damper bars eddy current losses (the heat sources of the damper bars) can be acquired.

B. THE DETAILS OF THE BOUNDARY VALUE PROBLEM OF THE ROTOR 3D TRANSIENT TEMPERATURE FIELD

In the construction of the rotor temperature field model, the following 2 key points have to be considered.

First, due to the existence of an air gap, the influence of the stator winding loss on the rotor's heat is neglected.

Secondly, the generator adopts symmetrical ventilation air cooling. As a result, due to the symmetric structure of the rotor pole and its ventilation system, the distribution of the rotor's temperature field is mirror-symmetric on both sides of the rotor shaft middle profile.

Therefore, half the axial section of the rotor, which consists of the rotor core, the damper bar, the field winding, and its bracket, *et al.*, is selected as the problem region for the 3D temperature field solving as shown in Fig. 3. There are 4 damper bars on each pole shoe. So, for an easier discussion, the damper bar on the leeward side is numbered as the 1st, and the damper bar on the windward side is numbered as the 4th.

Then, considering the anisotropic heat conduction condition of the rotor core, the boundary value problem of the 3D transient temperature field can be expressed as follows,

$$\begin{cases} \dfrac{\partial}{\partial x}(\lambda_x\dfrac{\partial T}{\partial x})+\dfrac{\partial}{\partial y}(\lambda_y\dfrac{\partial T}{\partial y})+\dfrac{\partial}{\partial z}(\lambda_z\dfrac{\partial T}{\partial z})+q_V=\rho c\dfrac{\partial T}{\partial t} \\ \lambda\dfrac{\partial T}{\partial n}\Big|_{S_A}=0 \\ \lambda\dfrac{\partial T}{\partial n}\Big|_{S_B}=-\alpha(T-T_f), \end{cases} \tag{A-1-11}$$

where T is the temperature, $\lambda_x, \lambda_y, \lambda_z$ represent the heat conductivity on each direction, respectively, q_v is the heat source density, which is obtained by the above-mentioned

multi-slice moving electromagnetic field-circuit coupling model of the generator, ρ is the density of the material, c is material specific heat, S_A represents the rotor middle profile and the interface between the rotor core and the rim related to the thermal insulation boundary condition, S_B is the outside surface of the rotor related to the heat dissipation boundary condition, α is the heat dissipation coefficient of S_B, and T_f is the environment air temperature.

According to the typical design manual of hydro-generators, the heat dissipation coefficients on the end and top surfaces of each pole shoe and the field winding can be calculated as follows, respectively, [1]:

$$\alpha = \frac{1 + 0.1\tau}{450} \quad \text{(A-1-12)}$$

$$\alpha'' = K\alpha', \quad \text{(A-1-13)}$$

where τ is the pole pitch, and K and α' are the coefficients related to the generator's structure, respectively.

Considering the better cooling conditions on the windward side, the heat dissipation coefficients of the pole shoe and the field winding are enlarged by certain proportion. On the contrary, the heat dissipation coefficients on the left side of the pole shoe and the field winding are reduced by certain proportion due to their worse cooling conditions.

On this basis, a time-step FE analysis of the 3D transient temperature field is carried out so the time-varying trend of the damper bar temperature can be obtained.

APPENDIX II
THE DETAILS OF VERIFICATION OF THE LOSS AND HEAT CALCULATIONS

Since short-circuit fault conditions can greatly damage the generator, it is not possible to intentionally let short-circuit faults take place to measure the temperature of the damper bar afterward. However, the initial state of modeling and analysis in this paper is the rated symmetrical operational state, namely the generator operating in the rated symmetrical state before the short circuit. In other words, for the 3D electromagnetic-temperature field transient analysis model established in this paper, while analyzing the short-circuit conditions, the first calculated generator state was the state before the occurrence of the short circuit, which is the rated symmetrical operational state. Therefore, by verifying the accuracy of the model's calculation of the damper bar temperature under the rated symmetrical operating state, the accuracy and rationality of the model's calculation of the damper bar loss and heat under the short-circuit condition can be indirectly or partially verified.

Since the studied tubular hydro-generator in this paper is operating in a hydropower station, and the station did not allow us to directly test the damper winding temperature. Consequently, in order to verify the accuracy of the model's calculation of the damper bar loss and heating under the rated conditions in this paper, we had to contact other hydropower stations to carry out the required measurements. Fortunately, one hydropower station agreed to our test request. Although this hydropower station had a vertical hydro-generator instead of a tubular one, the temperature measurement results of the damper bar of the vertical hydro-generator could indirectly verify the accuracy and rationality of the model in this paper.

Therefore,we tested the damper winding temperature of the vertical hydro-generator in that station and calculated its damper winding loss and temperature under the rated symmetrical condition using the present calculation model.

The generator operation conditions in the test are shown in TABLE 9.

TABLE 9. The generation operation condition in the test.

Parameter	Value
Active power (MW)	320
Stator voltage (kV)	17.4
Stator current (kA)	10.7
Rated power factor	0.9
Field voltage (V)	264
Field current (A)	1527

The temperature test was conducted using the MF51 semi-conductor thermistors, which are solid-pasted on the test points as shown in Fig. 15(a). In Fig. 15(b), the equipment in the positions 1–7 are listed in TABLE 10. In addition, a block diagram of the temperature test system is shown in Fig. 15(c). In this test system, infrared coding technology is adopted to transmit the signals between the rotor and the stator.

To prevent electromagnetic interference and protect the components of the temperature test, copper pipes were installed at some locations, including the rotor brackets on the surface of and inside the upper shaft.

Also, some test results are compared with the calculated results in TABLE 11.

TABLE 10. The eqeuipment in Fig. A-2-1. (B).

Position	Equipment
1	Static receiving component
2	Microcomputer temperature measuring instrument
3	Rotating transmitting component
4	Special wire clip and copper pipe
5	Special wire clip
6	The upper end shaft
7	The lead of temperature test components

TABLE 11. The verification of the damper winding temperature calculation.

Value	The test points				
	21#	23#	28#	29#	30#
Calculation value (℃)	29	31	42	44	47
Measured value (℃)	33	34	46	47	49
Error	−12.1%	−8.8%	−8.7%	−6.4%	−4%

The comparison between the above calculations and the measured values of the temperature at the test points shows that the results are similar.

It is worth noting that it is very difficult to directly measure the damper winding temperature for a number of reasons.

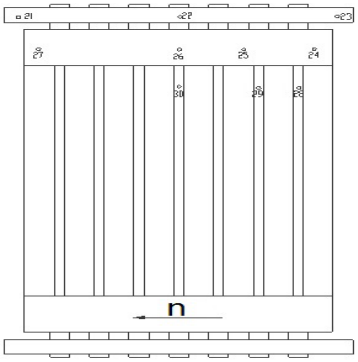

(a) The temperature test points of the damper winding

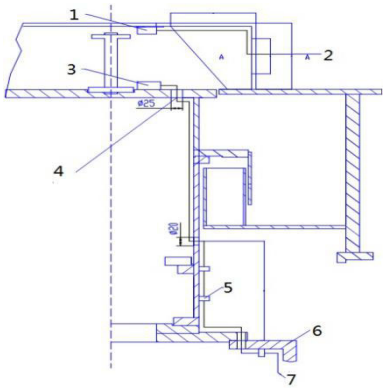

(b) The temperature test lead path

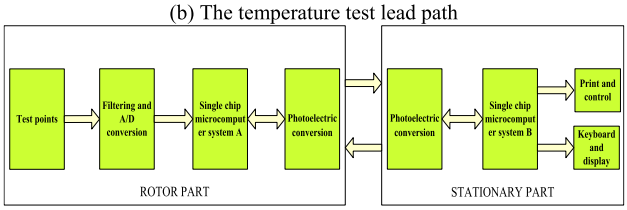

(c) The principle block diagram of the temperature test system

FIGURE 15. **The direct temperature test of the damper winding.**

First, it is difficult to install the temperature sensors in the damper bars. Second, the power supply of the measuring instrument is difficult. Third, due to the strong magnetic field in the generator, especially in the air gap, great interference takes place, which affects the signal transmission stability, making it difficult to ensure the integrity and accuracy of the measured temperature values. Fourth, the test costs are high. Especially for the tubular hydro-generator,due to the relatively small internal space,the damper winding temperature measurement is even more difficult [14], [15].

Due to the above reasons, as of now, Chinese generator manufacturing enterprises and power plants rarely carry out direct measurements of the damper winding temperatures of generators, especially of tubular hydro-generators.

Therefore, up till now, the above-measured values are our only on-site direct test data of the temperatures of the damper windings in hydro-generators. Although the tested generator is not the tubular hydro-generator with which we are concerned, the accuracy and rationality of our model can still be partially verified.

REFERENCES

[1] X.-F. Chen, *Electromagnetic Calculation of Hydro-Generator*. Beijing, China: China Water Power Press, 2011.

[2] C.-Y. Li, "The application of bulb-type hydro-generator set at low head hydropower station," *Developing*, no. 9, pp. 145–146, Sep. 2006.

[3] K. Weeber, "Determination of dynamic parameters of large hydro-generators by finite-element simulation of three-phase sudden short-circuit tests," in *Proc. IEEE Int. Electr. Mach. Drives Conf. Rec.*, May 1997, pp. MC1/13.1–MC1/13.3.

[4] R. Wamkeue, I. Kamwa, and X. Dai-Do, "Short-circuit test based maximum likelihood estimation of stability model of large generators," *IEEE Trans. Energy Convers.*, vol. 14, no. 2, pp. 167–174, Jun. 1999.

[5] R. Wamkeue, I. Kamwa, and M. Chacha, "Line-to-line short-circuit-based finite-element performance and parameter predictions of large hydro-generators," *IEEE Trans. Energy Convers.*, vol. 18, no. 3, pp. 370–378, Sep. 2003.

[6] Y. Xia, X. Yin, D. Chen, Z. Zhang, and W. Chen, "Transient simulation model and its simplified method validation for huge hydro generator internal short circuit faults," in *Proc. Int. Conf. Power Syst. Technol.*, Oct. 2006, pp. 1–5.

[7] Y. Fan, X. Wen, and S. A. K. S. Jafri, "3D transient temperature field analysis of the stator of a hydro-generator under the sudden short-circuit condition," *IET Electr. Power Appl.*, vol. 6, no. 3, pp. 143–148, Mar. 2012.

[8] C. Jing, L. Yan-ping, and Y. Qing-shuang, "The electromagnetic force calculation of damping windings under three-phase sudden short-circuit fault of large hydro-generator," in *Proc. 6th Int. Forum Strategic Technol.*, Aug. 2011, pp. 533–536.

[9] H. Jiawu, "Analysis of and reflection on the short-circuit fault of a large hydraulic generator," *IET Gener., Transmiss. Distrib.*, vol. 8, no. 4, pp. 661–669, Apr. 2014.

[10] J. Keränen, P. Ponomarev, J. Pippuri, P. Råback, M. Lyly, and J. Westerlund, "Parallel performance of multi-slice finite-element modeling of skewed electrical machines," *IEEE Trans. Magn.*, vol. 53, no. 6, pp. 1204–1207, Jun. 2017.

[11] A. M. Knight, S. Troitskaia, N. Stranges, and A. Merkhouf, "Analysis of large synchronous machines with axial skew, part 2: Inter-bar resistance, skew and losses," *IET Electr. Power Appl*, vol. 3, no. 5, pp. 398–406, 2009.

[12] Y. Huangfu, S. Wang, J. Qiu, H. Zhang, G. Wang, and J. Zhu, "Transient performance analysis of induction motor using field-circuit coupled finite-element method," *IEEE Trans. Magn.*, vol. 50, no. 2, pp. 2283–2286, Feb. 2014.

[13] A. Sarikhani, A. Nejadpak, and O. A. Mohammed, "Coupled field-circuit estimation of operational inductance in PM synchronous machines by a real-time physics-based inductance observer," *IEEE Trans. Magn.*, vol. 49, no. 5, pp. 2283–2286, May 2013.

[14] M. Bergeron, J. Cros, J. Niehenke, J. R. Figueroa, and C. Messier, "Hydro generator damper bar current measurement at wanapum dam," *IEEE Trans. Energy Convers.*, vol. 31, no. 4, pp. 1510–1520, Dec. 2016.

[15] H. Karmaker and A. M. Knight, "Investigation and simulation of fields in large salient-pole synchronous machines with skewed stator slots," *IEEE Trans. Energy Convers.*, vol. 20, no. 3, pp. 604–610, Sep. 2005.

QING-LING HU is currently pursuing the M.Sc. degree with Xihua University. His research interests include magnetic and thermal field calculation of generators, electrical machinery, and motor drives.

KE XIAO was born in Xuanhan, China, in 1992. He was graduated from Xihua University. His research interests include magnetic and thermal field calculation of generators, electrical machinery, and motor drives.

ZHI-TING ZHOU was born in Deyang, China, in 1999. She is currently pursuing the M.Sc. degree with Chongqing University. Her research interests include magnetic and thermal field calculation of generators, electrical machinery, and motor drives.

ZHEN-NAN FAN was born in Longchang, China, in 1981. He received the Ph.D. degree in electrical engineering from Chongqing University, Chongqing, China, in 2013. He is currently an Associate Professor with Xihua University. His research interests include magnetic and thermal field calculation of generators, electrical machinery, and motor drives.

YONG YANG was born in Hubei, China, in 1982. He received the bachelor's degree in electrical machine from Chongqing University, Chongqing, China, in 2006. He is currently a Senior Engineer with Dongfang Electric Machinery Company, Ltd. He is also involved in the electromagnetic analysis, calculation, and experimental research of electric machines.

ZU-YING BIAN is currently pursuing the M.Sc. degree with Xihua University. His research interests include magnetic and thermal field calculation of generators, electrical machinery, and motor drives.

JING-CAN LI was born in Yichang, China, in 1977. He received the Ph.D. degree in electrical engineering from Chongqing University, Chongqing, China, in 2011. He is currently a Lecturer with Chongqing University. His research interests include magnetic and thermal field calculation of generators, electrical machinery, motor drives, and the control of electrical machines.

BING YAO was born in Sichuan, China, in 1981. He received the M.Sc. degree from Xihua University, Chengdu, China, in 2010. He is currently a Lecturer with Xihua University. His research interests include magnetic and thermal field calculation of generators, electrical machinery, and motor drives.